

A 3D Ultrasound System for Medical Diagnosis

João Sanches¹, Jorge S. Marques¹ Fausto Pinto², and Paulo J. Ferreira³

¹ Instituto Superior Técnico, Instituto de Sistemas e Robótica
Torre Norte, Av. Rovisco Pais, 1049 Lisbon, Portugal

² Faculty of Medicine, University of Lisbon, Portugal

³ University of Aveiro, IEETA, Aveiro

Abstract. This paper presents a system for 3D ultrasound which aims to reconstruct a volume of interest from a set of ultrasound images. A Bayesian reconstruction algorithm has been recently proposed to perform this task. However, it is too slow to be useful in practice. This paper describes several techniques to improve the efficiency of the reconstruction procedure based multi-scale principles and based on the expansion of the likelihood function in a Taylor series. This allows the use of sufficient statistics which avoid processing all the images in each iteration and leads to a space-varying recursive filter designed according to the statistical properties of the data. Experimental results are provided to assess the performance of the proposed algorithms in medical diagnosis.

1 Introduction

Ultrasound is a non ionizing, non invasive and cheap medical imaging technology. Current systems, operating in B-scan mode, allow real time observation of cross sections of the human body. Several attempts have been made to extend ultrasound techniques in order to compute and visualize 3D representations of the human organs leading to three dimensional ultrasound systems [1].

Three dimensional ultrasound has several advantages with respect to classic ultrasound systems. First it provides new visual information since it allows the observation of the organs surface, as well as cross sections of the human body which can not be observed in B-scan mode, due to physical constraints. Second it provides quantitative measurements of volumes which can not be accurately obtained using standard B-scan mode. Both issues are important for medical diagnosis.

Three dimensional ultrasound can be performed either by using special types of probes, e.g. mechanical scanners which automatically sweep a region of interest by varying the inspection plane in a predefined way, or by using free hand scanning systems [1]. Mechanical scanners are simpler but they are more expensive and can only reconstruct small regions of the human body, while free hand scanners can be used to reconstruct larger regions. They require complex reconstruction algorithms though.

This paper describes a free-hand 3D ultrasound system. This system allows the estimation of a volume of data from a sequence of ultrasound images, corresponding to non parallel cross sections of the human body. This is a difficult

task since we have to estimate the whole volume from a finite number of noisy images, corrupted by speckle noise. The system must be able to perform noise reduction, to interpolate the data in regions which are not observed and also to compensate for the geometric deformations of the human organs during the data acquisition process. Bayesian techniques have been recently proposed to address these problems in a principled way but they are very time consuming [8] and can not be directly used in practice.

This paper describes several techniques to improve the efficiency of the reconstruction procedure based on multi-scale principles and on the expansion of the likelihood function in a Taylor series. This allows the use of sufficient statistics which avoid processing all the images in each iteration, leading to a space-varying recursive filter designed according to the statistical properties of the data. Experimental results are provided to assess the performance of the proposed algorithms in medical applications.

2 System Overview

This paper aims to reconstruct a volume of interest from a sequence of ultrasound images. The data acquisition system adopted in this work has three main components (see Fig.1),

- a medical ultrasound equipment with an ultrasound probe operating at 1.7 MHz.
- a spatial location system used for real time measurement of the probe position and orientation.
- a personal computer to capture the probe positions and ultrasound images at 25Hz rate, and reconstruct the volume.

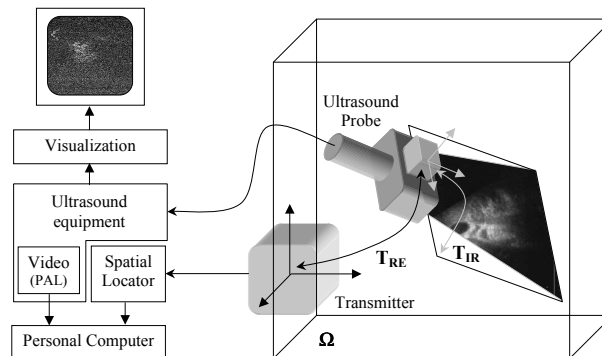


Fig. 1. Acquisition system.

During a medical exam a sequence of ultrasound images is provided, corresponding to non parallel cross sections of the human body. The probe position and

orientation, associated to each image, are also available. This allows to estimate the position of each pixel in 3D space, provided that we know the geometric transformation from the image coordinates into the probe coordinate system. This is estimated by a calibration procedure, similar to the single-wall calibration described in [13].

The volume of interest is reconstructed from the pixel intensities and positions, using a Bayesian reconstruction algorithm which is briefly described in section 3. This algorithm manages to interpolate the observed data, filling the gaps, and combines multiple observations to reduce the speckle noise. This is performed by adopting a parametric model for the function to be estimated, which depends on a large number of coefficients (many thousands), estimated using Bayesian techniques.

Visualization techniques (re-splicing, ray casting and thresholding) are used to display the results of the 3D reconstruction algorithm. All the software modules (data acquisition, sensor calibration, reconstruction and visualization) were developed in C++ in a Windows 2000 platform.

3 3D Reconstruction

Let $V = \{(x, y)_i\}$ the observed data after calibration, i.e., after the estimation of the transformation that relates the image coordinate system with the patient coordinate system. Each element of the vector V , contains the intensity, y_i and the corresponding 3D position, x_i , of each observed pixel from all images that form the sequence. This observed data is used to reconstruct the volume

Let consider the region to be estimated $\Omega \in R^3$ formed by a set of cubic cells called voxels.

The scalar function $f(x)$, describing the acoustic properties of the volume of interest, is obtained, inside each voxel, by interpolating the values of its vertices, i.e.,

$$f(x) = \Phi(x)^T U \quad (1)$$

where $\Phi(x) = \{\phi_1(x), \phi_2(x), \dots, \phi_n(x)\}$ is a vector of interpolation functions and $U = \{u_1, u_2, \dots, u_n\}$ a vector of intensity values associated to the grid nodes. The estimation of the volume is performed by estimating the vector U .

Each interpolation function is a separable function of the form $\phi_i(x) = \phi_i^1(x)\phi_i^2(x)\phi_i^3(x)$ where

$$\phi_i^j(x^j) = \begin{cases} (1 - \frac{d_i^j(x)}{\Delta}) & d_i^j(x) \leq \Delta \\ 0 & \text{otherwise} \end{cases} \quad (2)$$

Using the MAP method, the estimation of U is obtained by minimizing an energy function, i.e.

$$\hat{U} = \arg \min_U E(Y, X) \quad (3)$$

where $E(Y, X) = -l(V, U) - \log(p(U))$. $l(V, U) = \log(p(V|U))$ is the log likelihood function and $p(U)$ is the prior associated to the vector of nodes to estimate. The prior plays two important roles. First it allows to interpolate the data in points which were not observed, i.e., which do not belong to any observation plane. Second it improves the numerical stability of the iterative reconstruction algorithm.

Ultrasound images are very noisy being corrupted by multiplicative noise. A Rayleigh model is used in this paper to describe the observations. This noise, called *speckle*, is usually observed in process involving coherent radiation like LASER or SAAR.

It is assumed that the elements of Y are i.i.d. (independent and identically distributed) random variables with Rayleigh distribution ([2]),

$$p(y_i) = \frac{y_i}{f(x_i)} e^{-\frac{y_i^2}{2f(x_i)}} \quad (4)$$

where y_i denotes the amplitude of i -th pixel and $f(x_i)$ is the value of the function f computed at position x_i . The likelihood functions is generated by

$$l(V, U) = \sum_i \left\{ \log \left[\frac{y_i}{f(x_i)} \right] - \frac{y_i^2}{f(x_i)} \right\} \quad (5)$$

The statistical independence of all elements of V is assumed ([3]), despite the PSF (point spread function) of the image acquisition system be, in general, larger than the inter-pixel distance. In fact, it is not easy to estimate the PSF of the acquisition system. This function depends, not only on the impulsive response of the ultrasound probe and the associated electronics, but also on the image processing performed by ultrasound equipment. In particular, the filtering procedure that smoothes the original raw data by converting the polar grid of the RF signal to grid the image in cartesian coordinates introduces correlation among the pixels which is difficult to model. Furthermore, the improvement achieved in the reconstruction results by considering the statistical dependence among the pixels of the image is not relevant when compared with the computational complexity introduced in the algorithm, as noted by [4].

To derive $p(U)$ let us consider X as being a Markov random field. According the Hammersley-Clifford theorem, $p(U)$ is a Gibbs distribution. In this paper a Gibbs distribution with quadratic potential function is used

$$p(U) = \frac{1}{Z} e^{-\frac{\alpha}{N_v/2} \sum_{g,s} (u_g - u_g^s)^2} \quad (6)$$

where Z is a partition function, N_v is the number of neighbors of u_g , α is a parameter and u_g^s is the s -th neighbor of u_g (see details [7]). A 6-neighborhood system is considered in this paper. Note, that only half of the neighbors are considered in this summation to guarantee that each clique appears only once.

Using (5) and (6) leads to

$$E(V, U) = - \sum_i \left\{ \log \left[\frac{y_i}{f(x_i)} \right] - \frac{y_i^2}{f(x_i)} \right\} + \frac{\alpha}{N_v/2} \sum_{g,s} (u_g - u_g^s)^2 \quad (7)$$

The minimization of (7) with respect of U is a difficult task. The number of coefficients to estimate is of order of a million and $E(V, U)$ is a non convex function. To solve (3) the ICM algorithm, proposed by Besag is used [5]. In each iteration, the ICM algorithm minimizes the energy function with respect to only one variable, keeping all the others constant. To optimize (7) with respect to the variable u_n the following condition must be met

$$\frac{\partial E(V, U)}{\partial u_n} = 0 \quad (8)$$

which leads to

$$\frac{1}{2} \sum_i \frac{y_i^2 - 2f(x_i)}{f^2(x_i)} \phi_n(x_i) + 2\alpha N_v (u_n - \bar{u}_n) = 0 \quad (9)$$

where N_v is the number of neighbors of u_n , $\phi_n(x)$ is the interpolation function associated to the n-th node and $\bar{u}_n = \frac{1}{N_v} \sum_{j=1}^{N_v} (u_n)_j$ is the average value of the neighboring nodes of u_n .

This equation can be solved using the fixed point method leading to the next recursion expression

$$\hat{u}_n = \frac{1}{2\alpha N_v} \sum_i \frac{y_i^2 - 2f(x_i)}{f^2(x_i)} \phi_n(x_i) + \bar{u}_n \quad (10)$$

The solution of (3) using the ICM method leads to a set of non-linear equations, (9) which requires processing the pixels of the whole image sequence. Therefore, the reconstruction algorithm is computationally demanding and slow. To speed up the reconstruction process, several measures can be taken. In the next section three methods are proposed to simplify and speed up the solution of (10): i) a multi-scale approach, ii) the linearization of (10) allowing sufficient statistics and iii) a IIR filter to efficiently compute the MAP estimation of the volume.

4 Fast Algorithms

Three methods are considered to speed-up the reconstruction process. Detailed descriptions of these methods are published in [9, 10, 12].

Multi-scale The propagation of the information along the lattice due the prior is one of the main factors that slows down the convergence rate of the algorithm described in section 3. To overcome this difficulty, a multi-scale version is used. In this approach, coarse grids are used in the initial iterations being progressively refined until the final resolution is achieved. In this way, the long range interactions propagate fast in the first iterations speeding up the global convergence rate. In the last iterations the algorithm only performs small local adjustments. In this method the estimated volume obtained in a given iteration is used as starting point for the next iteration, and the resolution is doubled in consecutive iterations [9].

Linearization It is not possible to compute sufficient statistics associated to eqn (10) since he can not factorize the pdf. To obtain sufficient statistics a linearization of the likelihood function in the vicinity of the maximum likelihood estimate is performed. With this method, a small set of statistics computed in the initialization stage of the reconstruction algorithm and used along the whole optimization process. Therefore, the observations only have to be read from the disk and processed at the beginning. The observed data, compressed into a smaller number of coefficients, speeds up the processing time by more than one orders of magnitude [10]. The resulting equations are

$$\hat{u}_n = (1 - k_n)u_n^{ML} + k_n\bar{u}_n \quad (11)$$

$$u_n^{ML} = \frac{\sum_i y_i^2 \phi_n(x_i)}{\sum_i \phi_n(x_i)} \quad (12)$$

$$k_n = \frac{1}{1 + \frac{1}{4\alpha} \frac{\sum_i \phi_n(x_i)}{(u_n^{ML})^2}} \quad (13)$$

Filtering Equation (13) defines an IIR filter. This filter is not wedge supported [11]. Each output depends on past and future outputs since it depends on \bar{u}_p . Therefore, it is not possible to recursively compute the output in a single iteration. To overcome this difficulty we consider a set of eight wedge supported filters (see details on [12]), which can be recursively computed. The reconstructed volume is obtained by averaging the outputs of the eight wedge supported filters. This approach allows to improve the reconstruction time exploiting the computational efficiency of the recursive processing. With this methodology, reduction up to 25 times in the processing time can be achieved.

In this paper these three methods are used and combined into five different reconstruction strategies. They will be compared, using three figures of merit: the number of iterations, the processing time and the likelihood function. In the case of experiments using synthetic data a fourth figure of merit is also used: the signal to noise ratio. The methods considered in the experiments are

- | | |
|--------------|--|
| i) NLMAP-SS | Non multi-scale and non linear base algorithm. |
| ii) NLMAP-MS | Multi-scale and non linear base algorithm. |
| iii) LMAP-SS | Non multi-scale and linear algorithm. |
| vi) LMAP-MS | Multi-scale and linear algorithm. |
| v) IIRMAP | Recursive algorithm. |

5 Experimental Results

Experimental tests were carried out to evaluate performance of the five reconstruction techniques with synthetic and medical data using several figures of merit. Two examples are described in this section to illustrate the performance

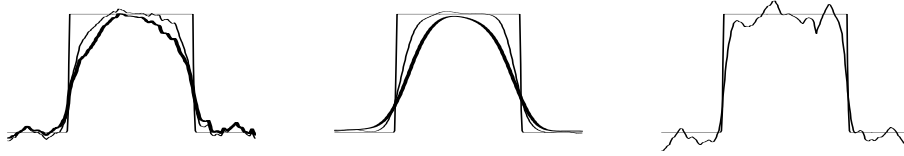


Fig. 2. Intensity profiles of the original and reconstructed volumes using i) NLMAP-SS and NLMAP-MS (bold); ii) LMAP-SS and LMAP-MS (bold); iii) IIRMAP

of the system with synthetic and medical data. More tests were performed but can not be included here due to space restrictions.

Synthetic Data This example considers the reconstruction of a binary function f defined as follows: $f(x) = A, \text{ if } x \in [-.5, .5]^3, f(x) = B, \text{ otherwise}$. Volume reconstruction is obtained from a set of 100 parallel cross-sections of the region $[-1, 1]^3$ corrupted by Rayleigh noise according to (4).

Figure 2 shows the intensity profiles of the original and reconstructed volumes along a given line. It is concluded that all the methods manage to estimate the original object reasonably well, showing some distortion at the transitions (blurring). The best transitions are obtained with the IIRMAP algorithm although this algorithm has the worst performance in stationary regions.

Table 1 shows four figures of merit which allow an objective comparison of several techniques in terms of SNR, final energy, iterations and computational effort. All methods manage to minimize the energy function and provide similar SNR results, except LMAP-MS which achieves worse results. The computational time is strongly dependent on the reconstruction method, the fastest reconstructions being achieved by the IIRMAP algorithm. The multi-scale approaches also achieve significant savings with respect to the single scale methods since they reduce the number of iterations. The fast algorithms reduce the computational effort of the NLMAP algorithm by 70 times (almost two orders of magnitude).

Method	Synthetic Data				Medical data		
	SNR (dB)	E ($\times 10^3$)	Time (s)	iterations	E ($\times 19^3$)	Time (s)	iterations
NLMAP-SS	20.1	8000.8	1534.53	64	8990.5	1893.4	96
NLMAP-MS	18.2	7999.5	403.32	17	8983.0	737.7	37
LMAP-SS	19.2	8000.8	298.17	36	9013.4	263.7	59
LMAP-MS	16.6	8002.5	113.63	9	8982.9	216.8	38
IIRMAP	20.4	8020.1	22.44	8	9156.3	21.4	8

Table 1. Results with synthetic and medical data

Medical Data Reconstruction tests were performed using the experimental setup described in section 2. This example shows the reconstruction of a gall

bladder from a set of 100 images corresponding to non parallel cross sections of the human body.

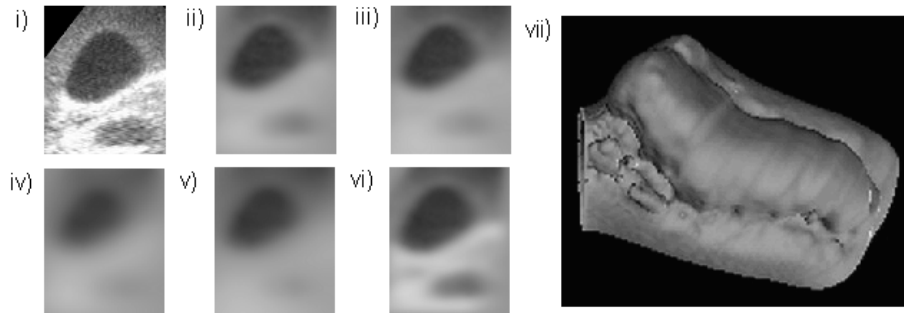


Fig. 3. Results with medical data: original cross section (i) and reconstructed cross sections obtained with ii) NLMAP-SS; iii) NLMAP-MS; iv) LMAP-SS; v) LMAP-MS; vi) IIRMAP; vii) Surface rendering of the gall bladder.

Figure 3 shows a cross section of the human body and the reconstructed results obtained by the five algorithms. These results are achieved by computing f along the inspection plane. Acceptable reconstruction results are obtained by all the algorithms. Table 1 shows the figures of merit associated to all the algorithms. Similar energy functions are obtained by all the methods, the best results being obtained by NLMAP-MS method.

Significant computational savings are achieved by using the fast algorithms, the fastest reconstruction being obtained by the IIRMAP method. The IIRMAP is 90 faster than the NLMAP algorithm. This can also be concluded from fig. 4 which displays the evolution of the energy during the optimization process as a function of the number of iterations. The surface of the gall bladder obtained with etdips 2.0 package is shown in Fig. 3.vii).

6 Conclusions

This paper considers the reconstruction of human organs from a set of ultrasound images, using five algorithms. A Bayesian approach is adopted in all these algorithms, leading to the optimization of an energy function which depends on a large number of variables (typically, a million variables). Two key ideas were explored: i) the use of multi-scale techniques which use coarse grids in the first iterations and finer grids afterwards and ii) a second order approximation of the energy function using the Taylor series. The Taylor series approach allows to reconstruct the volume of interest by low pass filtering the data with a space variant IIR filter, reducing the computational effort by almost two orders of magnitude. The best results were obtained by the IIRMAP method which provides a good trade off between accuracy and computational time.

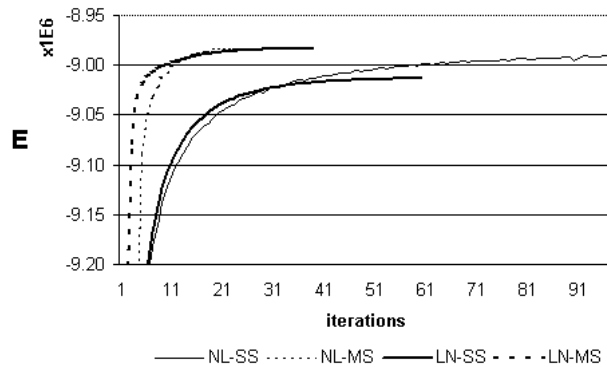


Fig. 4. Convergence 3D reconstruction methods i) NLMAP-SS; ii) NLMAP-MS; iii) LMAP-SS; iv) LMAP-MS; v) IIRMAP

References

1. T. Nelson, D. Downey, D. Pretorius, A. Fenster, Three-Dimensional Ultrasound, Lippincott, 1999.
2. Burckhardt C., Speckle in Ultrasound B-Mode Scans, IEEE Trans. on Sonics and Ultrasonics, vol. SU-25, no.1, pp.1-6, January 1978.
3. Dias J. and Leitão J., Wall position and thickness estimation from sequences of echocardiograms images, IEEE Transactions on Medical Imaging, vol.15, pp.25-38, February 1996.
4. E. Rignot and R. Chelappa, Segmentation of polarimetric synthetic aperture radar data, IEEE Trans. Image Processing, vol.1, no.1, pp. 281-300, 1992.
5. J. Besag, On the Statistical Analysis of Dirty Pictures, J. R. Statist. Soc. B, vol.48, no. 3, pp. 259-302, 1986.
6. R.W. Prager, R.N. Rohling, A.H. Gee and L. Berman. Rapid calibration for 3-D freehand ultrasound. Ultrasound in Medicine and Biology, 24(6):855-869, July 1998.
7. J.Sanches and J.S. Marques, A Rayleigh reconstruction/interpolation algorithm for 3D ultrasound, Pattern Recognition Letters, 21, pp. 917-926, 2000.
8. J.Sanches and J.S. Marques, Joint Image Registration and Volume Reconstruction for 3D Ultrasound, Special Issue on 3D Ultrasound, Pattern Recognition Letters (Aceite).
9. J.Sanches and J.S. Marques, A Multi-Scale Algorithm for three dimensional Free Hand Ultrasound, Ultrasound in medicine and biology, Elsevier (Aceite).
10. J.Sanches and J.S. Marques, A Fast MAP Algorithm for 3D Ultrasound, Proceedings Third International Workshop on Energy Minimization Methods in Computer Vision and Pattern Recognition, Sophia Antipolis, France, pp. 63-74, September 2001.
11. Jae. S. Lim, Two-Dimensional Signal and Image Processing, PTR Prentice Hall, Englewood Cliffs, New Jersey.
12. J.Sanches and J.S. Marques, A MAP Filter for 3D Ultrasound, Proceedings IEEE International Conference on Image Processing, Rochester-NY, USA, September 2002 (Aceite).
13. R.W.Prager, R.N.Rohling, A.H.Gee and L.Berman, Automatic Calibration for 3-D Free-Hand Ultrasound, Cambridge University, CUED/F-INFENG/TR 303, September 1997.